Supporting Information

Ultra-stable multi-shell blue-emissive $CsPbBr_3$ nanoplatelets with enhanced performance through chelating ligand and silica passivation

Yating Fan[1], Tianfeng Li[1†], Mengyao Kou[1], Zihao Song[1], Lizhen Gao[2†], Yanmin Kuang[1], Xiaojuan Wang[1], and Lijun Guo[2]

[1]School of Physics and Electronics, International Joint Research Laboratory of New Energy Materials and Devices of Henan Province, Henan University, Kaifeng 475004, China.

E-mail: litianfeng@henu.edu.cn

[2]Henan Key Laboratory of High Efficiency Energy Conversion Science and Technology, School of Physics and Electronics, Henan University, Kaifeng 475004, China.

E-mail: gaolizhen@henu.edu.cn

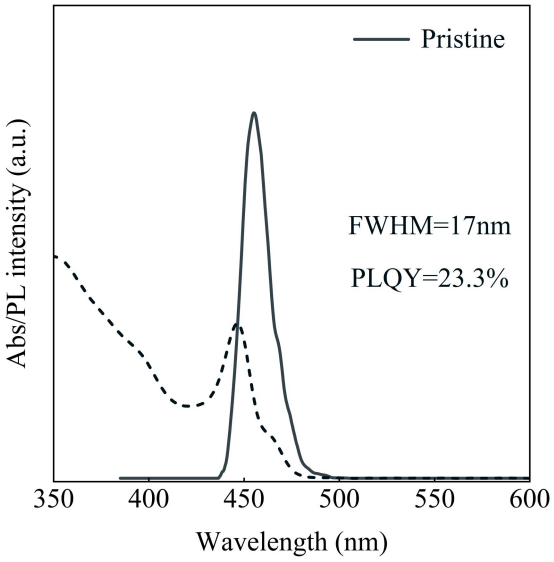


Fig. S1. UV-Vis absorption spectra (dashed curve) and PL spectra (solid curve) of pristine $CsPbBr_3$ nanoplatelets.

The PL spectra deliver a narrow emission band with a FWHM of 17 nm around 455 nm, demonstrating narrow size dispersion of the nanoplatelet products[1]. The corresponding photoluminescence quantum yield (PLQY) of the pristine $CsPbBr_3$ nanoplatelets is measured to be 23.3%. A well-defined excitonic absorption band is observed from the dashed absorption trace, matching the position of the dominant PL emission maximum at approximately 455 nm.

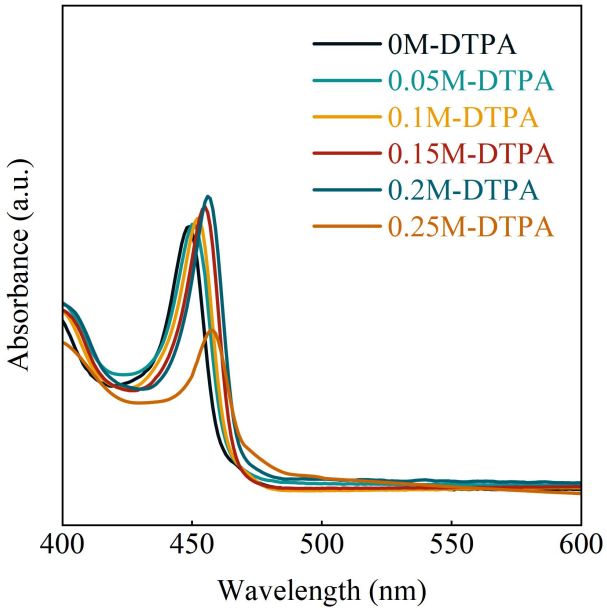


Fig. S2. UV-Vis absorption spectra of $CsPbBr_3$ nanoplatelets before and after DTPA treatment with different concentrations.

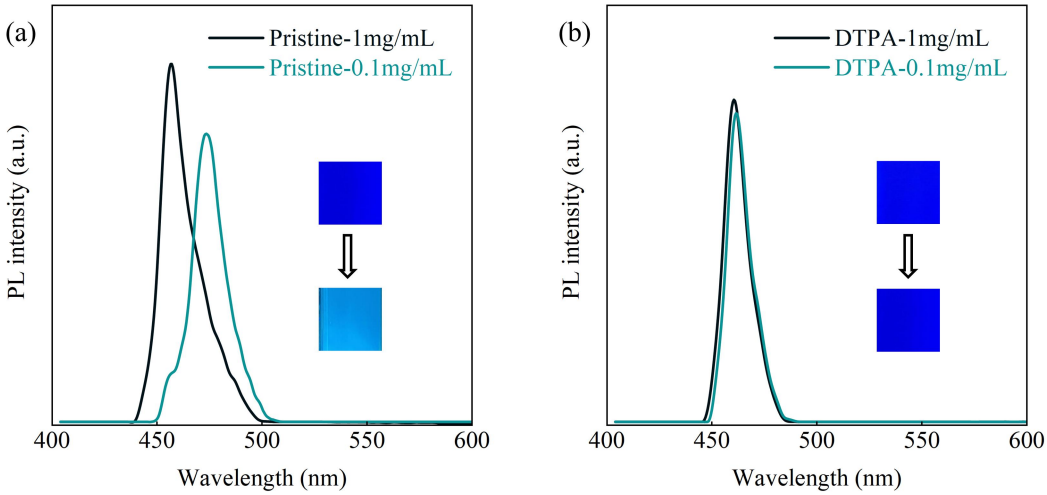


Fig. S3. (a, b) PL stability of the pristine NPLs and DTPA NPLs treated with deep dilution.

Upon deep dilution of NPLs, the photoluminescence (PL) peak position remained stable in DTPA-based NPLs. In contrast, the PL peak from pristine NPLs shifted to the green band due to the dissociation of surface ligands (Fig. S3). These results further support the conclusion that DTPA with 8 chelating sites exhibits stronger adhesion to the NPL surface, thereby enhancing their stability[2].

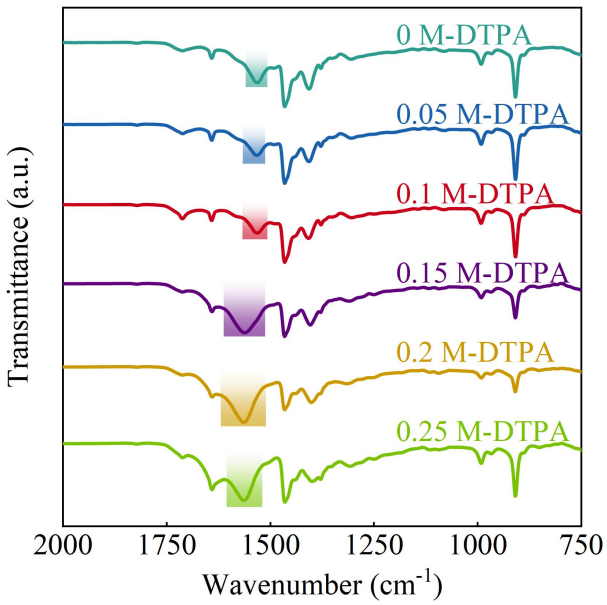


Fig. S4. FTIR transmittance spectra of $CsPbBr_3$ nanoplates (NPLs) modified with varying concentrations of DTPA.

Two characteristic absorption bands in the range of 1650-1540 cm^{-1} and 1450-1360 cm^{-1} are assigned to the asymmetric and symmetric stretching vibrations of carboxylate groups ($-COO^-$), which confirms the successful immobilization of DTPA on the NPL surface[3]. The 0 M DTPA bare sample exhibits weak absorption signals at these two wavenumbers. As DTPA concentration increases from 0.05 to 0.2 M, the intensities of the two carboxylate peaks gradually enhance and hit the maximum value at 0.2 M. These phenomena demonstrate that DTPA coordinates with surface Pb^{2+} ions via carboxyl groups, and the coordination degree shows a positive correlation with surface passivation efficiency.

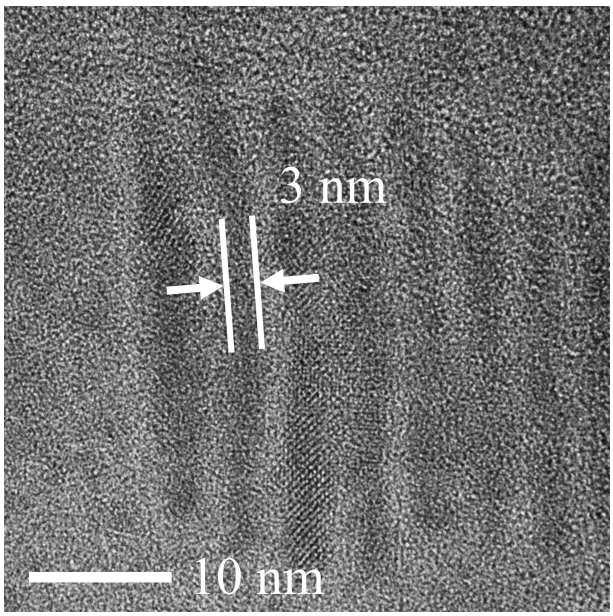


Fig. S5. TEM image of DTPA-Mn^{2+} NPLs.

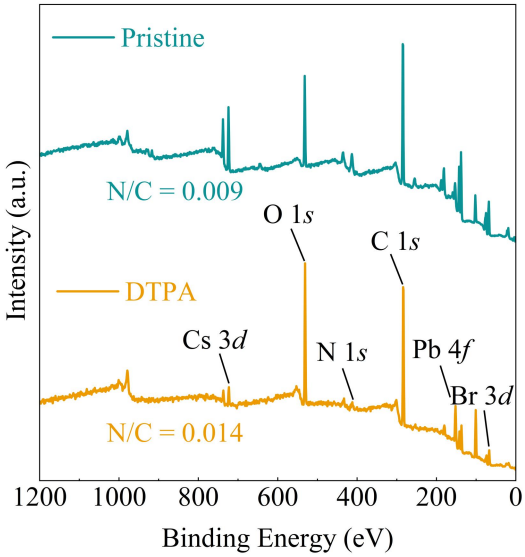


Fig. S6. Survey XPS spectra of the pristine NPLs and DTPA-NPLs. Short lines mark the expected binding energy positions of core-level characteristic peaks for Cs 3*d*, Pb 4*f*, Br 3*d*, C 1*s*, N 1*s*, and O 1*s*.

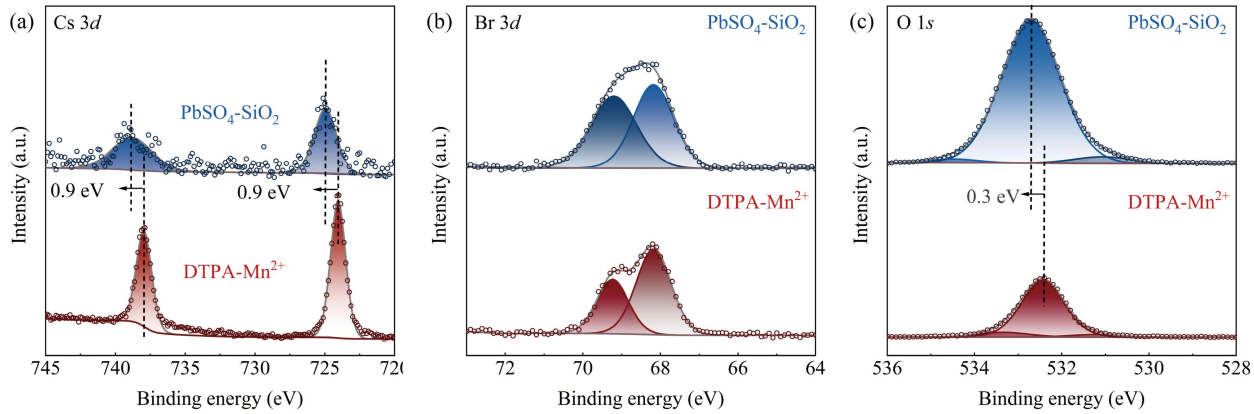


Fig. S7. High-resolution XPS spectra of $PbSO_4$-SiO_2 NPLs and DTPA-Mn^{2+} NPLs: (a) Cs 3*d*, (b) Br 3*d* and (c) O 1*s*.

The N/C atomic ratio calculated quantitatively from the survey XPS spectra is 0.009 for pristine NPLs and 0.014 for DTPA-NPLs. Note: XPS only probes a region of several nanometers at the sample surface. The obtained atomic ratios are semi-quantitative and susceptible to adventitious carbon contamination. These values are only used for trend analysis of surface ligand variations.

The characteristic peaks of Cs 3*d*, Br 3*d* and O 1*s* for $PbSO_4$-SiO_2-NPLs exhibit obvious shifts toward higher binding energies relative to the DTPA-Mn^{2+} counterparts. The increased binding energies reveal electron transfer from the $CsPbBr_3$ perovskite matrix to the outer $PbSO_4$-SiO_2 shell, verifying strong interfacial electronic interaction and stable chemical bonding between the inorganic coating and perovskite nanoplates[4].

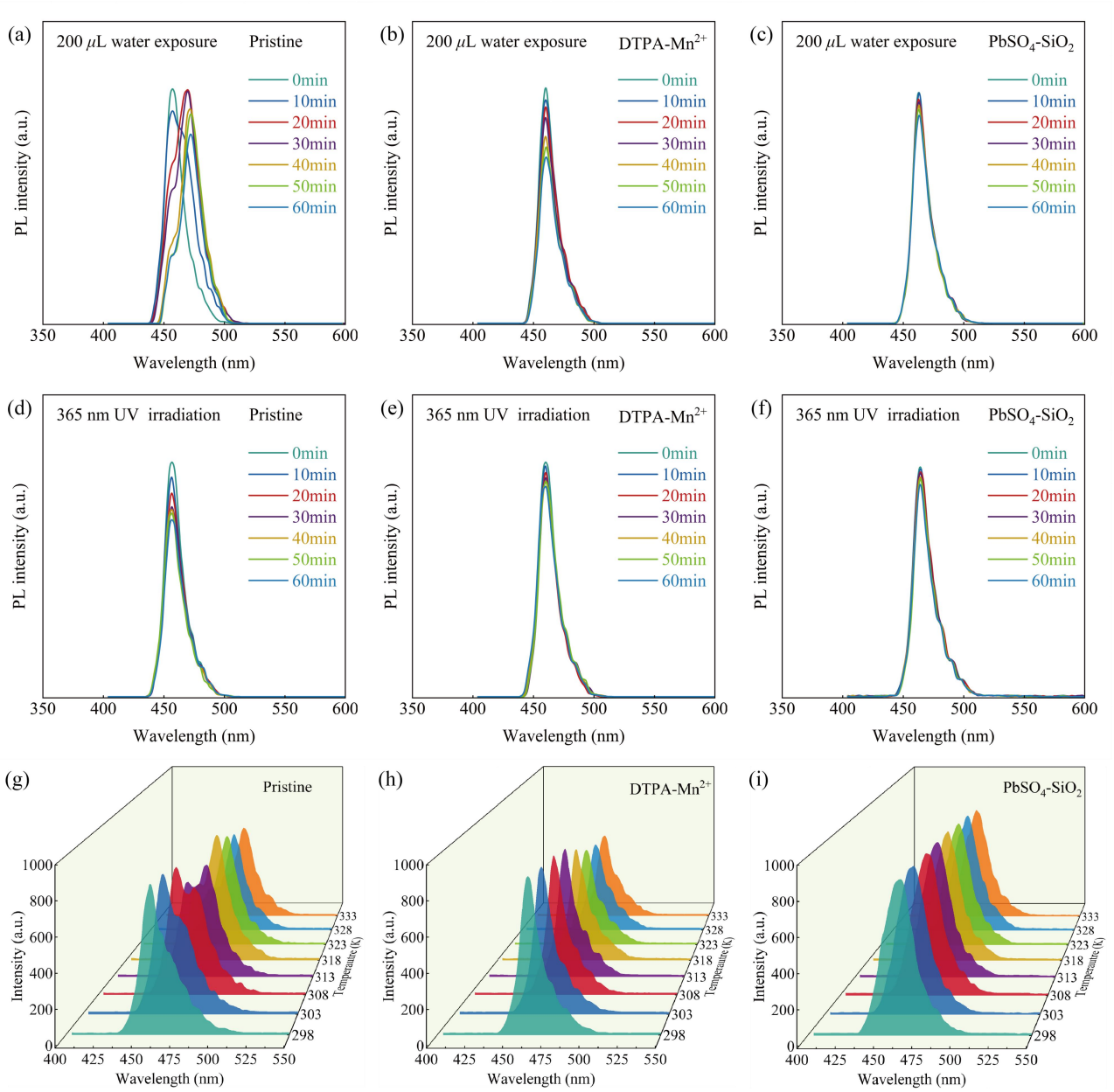


Fig. S8. Normalized PL intensity evolution reflecting stability of pristine, DTPA-Mn^{2+}-NPLs, and $PbSO_4$-SiO_2-NPLs under different aging conditions: (a-c) Water exposure, (d-f) UV irradiation and (g-i) continuous heating at 60 °C.

Table S1 Double-exponential-fitted PL lifetime data of $CsPbBr_3$ NPLs passivated with gradient DTPA concentrations.

DTPA (M)	A_1(%)	τ_1(ns)	A_2(%)	T_2(ns)	τ_{avg}(ns)
0	80.48	1.503	20.26	5.916	3.700
0.05	88.77	1.887	17.65	6.960	3.033
0.1	72.06	1.526	29.17	5.686	4.027
0.15	77.19	2.260	26.75	6.734	4.533
0.2	59.09	1.393	38.16	6.300	5.048
0.25	84.72	1.175	19.05	6.732	4.303

Table S2 Double-exponential-fitted PL lifetime data of $CsPbBr_3$ NPLs under diverse surface modification strategies.

	A_1(%)	τ_1(ns)	A_2(%)	T_2(ns)	τ_{avg}(ns)
Pristine	80.48	1.503	20.26	5.916	3.700
Mn^{2+}	73.06	1.706	35.21	5.577	4.074
DTPA	59.09	1.393	38.16	6.300	5.048
DTPA-Mn^{2+}	35.93	2.393	60.94	7.503	6.694
$PbSO_4$-SiO_2	53.48	4.336	41.72	12.59	10.06

To elucidate the mechanism of doping-induced luminescence enhancement, the bulk fluorescence lifetime of the samples was measured using a fluorescence lifetime spectrometer, which records the arrival time of individual photons to construct the fluorescence decay curve. The decay curve was fitted using a double-exponential function (Equation 1), and the average fluorescence lifetime was calculated via (Equation 2):

$$I(t) = A_1 * \exp\left(-\frac{t}{\tau_1}\right) + A_2 * \exp\left(-\frac{t}{\tau_2}\right) \quad (1)$$

$$\tau = \frac{A_1 * \tau_1^2 + A_2 * \tau_2^2}{A_1 * \tau_1 + A_2 * \tau_2} \quad (2)$$

The pristine sample exhibited the fastest fluorescence decay and the shortest lifetime. After DTPA modification, the 0.2 M DTPA-treated group had the longest lifetime, while the lifetime decreased sharply at 0.25 M, excessive DTPA weakened the passivation effect and accelerated non-radiative recombination. After treatment with $PbSO_4$-SiO_2, an impressive PL lifetime of up to 10.06 ns is achieved. The prolonged lifetime confirms that $PbSO_4$-SiO_2 and DTPA effectively passivated surface defects, suppressed non-radiative recombination, and promoted radiative recombination as the dominant photophysical process.

Table S3 Radiative (K_r) and non-radiative (K_{nr}) recombination rate data of $CsPbBr_3$ NPLs passivated with gradient DTPA concentrations.

DTPA (M)	PLQY (%)	K_r(ns^{-1})	K_{nr}(ns^{-1})	K_r/K_{nr}
0	23.3	0.063	0.207	0.304
0.05	25.1	0.083	0.247	0.335
0.1	28.9	0.072	0.177	0.406
0.15	32.5	0.072	0.149	0.481
0.2	55.7	0.110	0.088	1.257
0.25	18.3	0.043	0.189	0.224

Table S4 Radiative (K_r) and non-radiative (K_{nr}) recombination rate data of $CsPbBr_3$ NPLs under diverse surface modification strategies.

	PLQY (%)	K_r(ns^{-1})	K_{nr}(ns^{-1})	K_r/K_{nr}
Pristine	23.3	0.063	0.207	0.304
Mn^{2+}	52.3	0.128	0.117	1.096
DTPA	55.7	0.110	0.088	1.257
DTPA-Mn^{2+}	82.5	0.123	0.026	4.714
$PbSO_4$-SiO_2	90.6	0.090	0.009	9.638

The radiative recombination rate (K_r), non-radiative recombination rate (K_{nr}), and their ratio (K_r/K_{nr}) were further calculated from the PLQY and fluorescence lifetime data using (Equation 3) and (Equation 4):

$$\frac{1}{\tau_{avg}} = K_r + K_{nr} \tag{3}$$

$$\eta_{PLQY} = \frac{K_r}{K_r + K_{nr}} \tag{4}$$

As listed in Table S4, the K_r/K_{nr} ratio of the $PbSO_4$-SiO_2-NPLs sample exhibited a remarkable 32-fold enhancement relative to the pristine NPLs. The prominent enhancement in the radiative-to-nonradiative recombination rate ratio indicates that the photophysical behavior of the composite samples is dominated by radiative recombination. Consequently, the synergistic effect of $PbSO_4$-SiO_2 composite structure construction and DTPA surface passivation greatly reduce the surface defect density of perovskite nanoplatelets, suppresses trap-mediated nonradiative recombination pathways, and ultimately realizes the predominant radiative recombination process.

Table S5 XPS atomic percentages of elements for pristine and DTPA $CsPbBr_3$ NPLs.

Atomic (%)	Cs 3*d*	Pb 4*f*	Br 3*d*	O 1*s*	C 1*s*	N 1*s*	N/C
Pristine	1.48	1.12	3.71	12.79	52.28	0.49	0.009
DTPA	0.15	0.16	0.60	7.07	19.85	0.28	0.014

References

[1]Song Y, Cao S, Wang Y, et al. Efficient deep-blue LEDs based on colloidal $CsPbBr_3$ nanoplatelets meeting the Rec.2020 standard. Light: Science & Applications, 2025, 14(1): 336

[2]Liu Y, Shao X, Gao Z, et al. In situ and General Multidentate Ligand Passivation Achieves Efficient and Ultra-Stable $CsPbX_3$ Perovskite Quantum Dots for White Light-Emitting Diodes. Small, 2023, 20(3): 2305664

[3]Lin H, Gao P L, Dong J Y, et al. Bi-Functional Chelating Ligand Enables Ultra-Stable Blue Emissive $CsPbBr_3$ Nanoplatelets Film. Advanced Optical Materials, 2024, 12(19): 2400214

[4]Tang Y, Zhang X, Liao K, et al. Ultra-Stable Perovskite Quantum Dot Polymer Films. Advanced Optical Materials, 2024, 13(10): 2402688